46th Annual Review of Progress
in Quantitative Nondestructive Evaluation
QNDE2019
July 14-19, 2019, Portland, OR, USA

QNDE2019-???

TERAHERTZ DEFECT EVALUTION IN OXIDE/OXIDE CERAMIC MATRIX COMPOSITES

John Nagel[1], Chien-Ping Chiou[1], Leonard Bond[1] and Waled Hassan[2]
[1]Center for Nondestructive Evaluation, Iowa State University, Ames, IA
[2]Rolls-Royce North America, Indianapolis, IN 46225

ABSTRACT

Pulsed terahertz imaging was used to inspect several oxide/oxide ceramic matrix composite samples. A data processing framework was created in order to detect test defects that were imbedded in the samples. Signal and imaging processing techniques were used in order to process the data, automatically detect defects, and calculated the signal-to-noise ratio was calculated for all detected defects. The detection performance between C-Scan images that were constructed using a single wide time gate and multiple narrow time gates are examined. We used the signal processing technique of spatial signal averaging was also used to remove deterministic interference in the sample that was present as the result of multi-layer reflections and water vapor. The effect of the removal of the deterministic interference on the signal-to-noise ratios is presented and discussed.

Keywords: terahertz, ceramic matrix composite, image processing

NOMENCLATURE

THz	terahertz
CMC	ceramic matrix composite
ox/ox	oxide/oxide
SNR	signal-to-noise ratio

1. INTRODUCTION

Ceramic matrix composites (CMC's) are currently in development for use in next generation aircraft engines to help meet the increasing demands of power efficiency while saving weight. A subset of CMC's is oxide-oxide CMC's, which are generating interest for materials to manufacture aircraft engine structural components and exhaust systems [1]. As with most composites, delaminations, cracking, and porosity pose problems for ceramic composites [2]. As a result, testing of these materials will be vital to the future safety of many products. Several methods of nondestructive testing (NDT) have already been studied for the inspection of CMC's including flash thermography [1, 3], ultrasound, X-Ray, and impact acoustic resonant spectroscopy [3]. Recently, terahertz imaging has been a proposed method for evaluating the integrity of ceramic matrix composites. Terahertz has advantages over traditional methods such as X-Rays in that it is nonionizing and traditional ultrasound in that in that it does not require a coupling medium.

Terahertz (THz) is electromagnetic radiation residing in the frequency range between microwave and infrared. Commonly considered to consist of the region from about 0.1 THz (3 mm) to 10 THz (30 µm), it has greater penetration depth than infrared light and better resolution than microwaves due to its shorter wavelength. THz is able to penetrate many non-conducting materials, such as glasses, plastics, and ceramics and thus is an applicable method for investigating many structural materials. Several authors have already been able to use terahertz radiation for the inspection of CMC's. Continuous Wave THz has been used to locate delaminations [4], while THz time-domain spectroscopy (THz-TDS) has been used to detect damage in SiNC CMC's [5]. THz-TDS data from a CMC inspection has even served as the input to a machine learning algorithm for detecting delaminations [6].

In this study we will be describing an algorithm that was constructed to locate embedded flaws in four test samples of oxide-oxide CMCs that were inspected using THz-TDS. In addition, we will discuss several methods to improve defect detection along with the removal of some of the material noise that is present when inspecting a layered material system with THz-TDS along with its impact on the signal-to-noise ratio of the detected flaws.

2. MATERIALS AND METHODS

The terahertz time domain spectroscopy (THz-TDS) system used in this study was custom built based on the TPI-Imaga 2000 model manufactured by Teraview Ltd. The transmitter and receiver pair implement photoconductive dipole antennas driven by a femtosecond titanium-sapphire laser. The transmitter generates a THz pulse with a bandwidth ranging from approximately 50 GHz to 4 THz and has full-width-half-maximum spot size at focus of 800 µm. The system also contains a mechanical gantry that is capable of raster-scanning in both the x and y-axes which allows for the creation of two-dimensional images from some characteristic of the THz waveform that is captured at each point.

We had access to four samples of oxide-oxide CMC's each embedded with metal inclusions and intentional delaminations of varying sizes and depths for test defects. Two of the CMC's were 6" x 6" and the other two were 9" x 9" with each size containing a sample that was 5 and 12 plies thick.

2.1 Methodology

The CMC samples were scanned by the THz system using a rectangular grid with a spacing between data points of 500 µm in both the x and y axes. Each sampling point consisted of an A-Scan that was 60ps in length. The C-Scan image that will be the focus of this work was generated by considering the peak-to-peak amplitude of each THz A-Scan between two specified points in time, what will be called a time gate. The C-Scan image for each sample will be the media from which the embedded defects are located and a signal-to-noise ratio (SNR) is generated

This study compares two different time gate methods of generating the C-Scan image for each sample. The first is known as the wide gate and involves setting the time gate between the front and back surface echoes of the on each A-Scan, effectively creating a time gate that considers the entire inside of the sample. The other method is the multiple narrow gate method, where a series of time gates and C-Scans are generated for each sample. The wide gate method has the advantage of being simple and efficient while the narrow gate method uses only parts of the sample that are around the same depth, considerably reducing the noise level. An example of an A-Scan with the wide time gate is shown in Figure 1, while an example of a narrow time gate is shown in Figure 2.

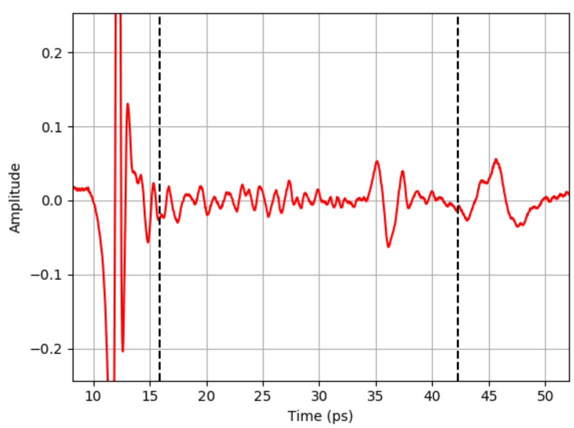

FIGURE 1: EXAMPLE OF AN A-SCAN SHOWING THE WIDE TIME GATE. THE DASHED BLACK LINES REPRESENT THE TIME GATE.

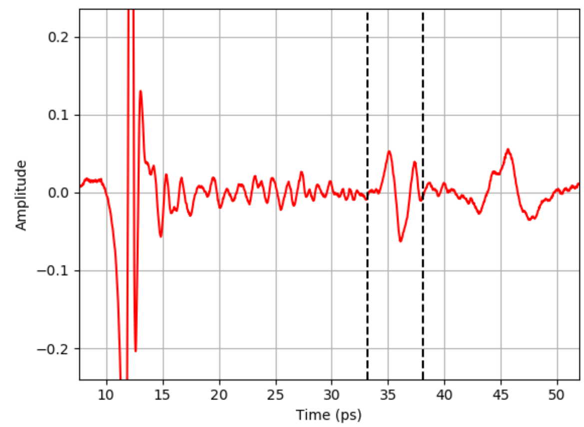

FIGURE 2: EXAMPLE OF AN A-SCAN SHOWING A NARROW TIME GATE WHERE THE BLACK DASHED LINES REPRESENT THE TIME GATE.

Regardless of the time gate that is used to generate the C-Scan image, the result will be an image with a few visible defects scattered throughout. These defects can be segmented out of the image with a binary thresholding function. In this work, the triangle threshold was chosen. It was first introduced in a paper by Zack et al. [1] and is a histogram based thresholding method useful for separating a small tail of pixels from a large region of background region. A pictorial description of the thresholding algorithm is shown in Figure 3.

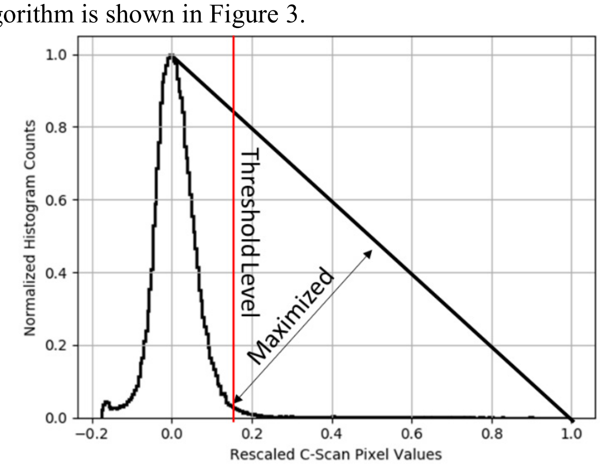

FIGURE 3: DESCRIPTION OF THE TRIANGLE THRESHOLD ALGORITHM THAT WAS USED IN THIS WORK.

When inspected with THz-TDS the CMC samples generate a significant amount of deterministic interference. There are many reverberations of the THz wave in between the layers that make up the sample. In addition, there is also water vapor interference that is often present in the THz spectral range. Therefor we seek to remove as much of this deterministic interference as possible by using a spatial averaging technique and subtracting the generated waveform that represents the "average" response of the sample under study. The result that is left will be, as best as possible, the truly random nature of the THz response to the sample and provide the most accurate calculation of the SNR.

A secondary SNR threshold was also used in this study to reduce the number of false alarms. This was applied after the triangle threshold described above.

3. RESULTS AND DISCUSSION

After the data has been processed as described in the previous section the SNR is calculated for all of the possible defects indicated by the triangle threshold using the definition below.

$$SNR = \frac{P_s - \mu_n}{P_n - \mu_n} \quad (1)$$

In Equation 1, P_s represents the largest amplitude of a flaw signal in the image, P_n is the largest noise amplitude and μ_n is the average noise amplitude. This equation is commonly used in NDE applications to determine the detectability of defects in images [8, 9].

After applying an SNR threshold to the data, the number of detected flaws and false alarms based on a map of the defects are calculated. It was found that removing the deterministic interference resulted in less false alarms and generally a higher SNR for the detected flaws. An example of a C-Scan image with some of the detected flaws and false alarms is shown in Figure 4.

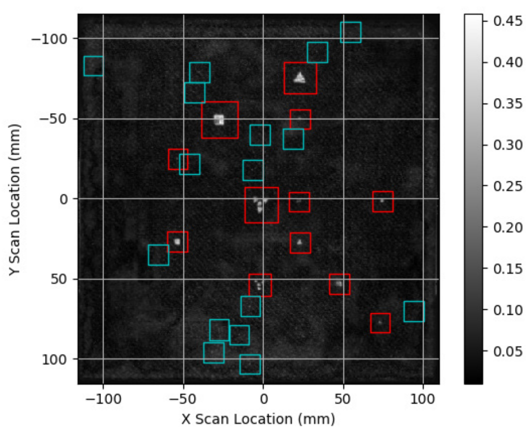

FIGURE 4: AN EXAMPLE OF THE DETECTION OF DEFECTS AND SEVERAL FALSE ALARMS IN ONE OF THE C-SCAN IMAGES GENERATED FOR SAMPLE 3.

4. CONCLUSION

In this work a data processing procedure was developed for the automatic detection of embedded test defects in four oxide/oxide CMC samples. It was found that a series of narrow time gates produced better results in terms of defect detection than a single wide time gate set to encompass the entire volume of the material under question. The removal of deterministic noise also allows for better defect detection and generally improves the SNR of defects in the thicker samples.

ACKNOWLEDGEMENTS

The authors would like to thank Rolls-Royce North America for providing the samples. We would also like to thank Dr. Waled Hasan, Mr. Joe Henderkott and Ms. Sunny Chang for useful discussion on the work.

REFERENCES

[1] Michael J. Walock, Vann Heng, Andy Nieto, Anindya Ghoshal, Mathuval Murugan, and Dan Driemeyer, "Ceramic Matrix Composite Materials for Engine Exhaust Systems on Next-Generation Vertical Lift Vehicles," *Journal of Engineering for Gas Turbine and Power*, Vol. 140 No. 10 (2018): 102101. DOI 10.1115/1.4040011.

[2] Y. Gowayed, G. Ojard, E. Prevost, U. Santhosh, G. Jefferson, "Defects in ceramic matrix composites and their impact on elastic properties", *Composites Part B: Engineering*. Vol. 55 (2013): pp. 167-175 DOI 10.1016/j.compositesb.2013.06.026

[3] J. G. Sun, C. M. Deemer, W. A. Ellingson, and J. Wheeler, "NDT Technologies for Ceramic Matrix Composites: Oxide and Non-Oxide," *Materials Evaluation*, Vol. 64 No. 1 (2006). pp. 52-60.

[4] S. Becker, T. Ullmann, and G. Busse. "3D Terahertz Imaging of Hidden Defects in Oxide Fibre Reinforced Ceramic Composites." *4th International Symposium of NDT in Aerospace*, 2012

[5] L. Owens. "Characterization of Ceramic Composite Materials Using Terahertz Non-Destructive Evaluation Techniques." MS Thesis. Wright State University, Dayton, OH. 2012.

[6] J. Ren, L. Li, D. Zhang, X. Qiao, Q. Lv, and G. Cao. "Study on intelligent recognition detection technology of debond defects for ceramic matrix composites based on terahertz time domain spectroscopy." *Applied Optics*. Vol. 55 No. 26 (2016) pp. 7204-7211. DOI 10.1364/AO.55.007204

[7] Zack, Gregory W., Rogers, William E., and Latt, Samuel A. "Automatic Measurement of Sister Chromatid Exchange Frequency." *The Journal of Histochemistry and Cytochemistry* Vol. 25 No. 7 (1977): pp. 741-753. DOI 10.1177/25.7.70454.

[8] P. J. Howard, D. C. Copley, and R. S. Gilmore. "A Signal-to-Noise Ratio Comparison of Ultrasonic Transducers for C-Scan Imaging in Titanium." *Review of Progress in Quantitative Nondestructive Evaluation, Vol. 14*. pp. 2113-2120.

[9] Li, Ming, Holland, Stephan D., and Meeker, William Q. "Statistical methods for automatic crack detection based on vibrothermography sequence-of-images data." *Applied Stochastic Models in Business and Industry*. Vol. 26 No. 5 (2010): pp. 481-495. DOI 10.1002/asmb.866.